

Article

# Similarity Theory Based Radial Turbine Performance and Loss Mechanism Comparison between R245fa and Air for Heavy-Duty Diesel Engine Organic Rankine Cycles

Lei Zhang<sup>1</sup>, Weilin Zhuge<sup>1,2</sup>, Yangjun Zhang<sup>1,2,\*</sup> and Tao Chen<sup>1</sup>

<sup>1</sup> State Key Laboratory of Automotive Safety and Energy, Tsinghua University, Beijing 100084, China; zlei11@mails.tsinghua.edu.cn (L.Z.); zhugewl@tsinghua.edu.cn (W.Z.); t-chen14@mails.tsinghua.edu.cn (T.C.)

<sup>2</sup> Collaborative Innovation Center of Electric Vehicles in Beijing, Beijing 100081, China

\* Correspondence: yjzhang@tsinghua.edu.cn; Tel.: +86-10-6279-7359

Academic Editor: Brian Agnew

Received: 13 November 2016; Accepted: 5 January 2017; Published: 14 January 2017

**Abstract:** Organic Rankine Cycles using radial turbines as expanders are considered as one of the most efficient technologies to convert heavy-duty diesel engine waste heat into useful work. Turbine similarity design based on the existing air turbine profiles is time saving. Due to totally different thermodynamic properties between organic fluids and air, its influence on turbine performance and loss mechanisms need to be analyzed. This paper numerically simulated a radial turbine under similar conditions between R245fa and air, and compared the differences of the turbine performance and loss mechanisms. Larger specific heat ratio of air leads to air turbine operating at higher pressure ratios. As R245fa gas constant is only about one-fifth of air gas constant, reduced rotating speeds of R245fa turbine are only 0.4-fold of those of air turbine, and reduced mass flow rates are about twice of those of air turbine. When using R245fa as working fluid, the nozzle shock wave losses decrease but rotor suction surface separation vortex losses increase, and eventually leads that isentropic efficiencies of R245fa turbine in the commonly used velocity ratio range from 0.5 to 0.9 are 3%–4% lower than those of air turbine.

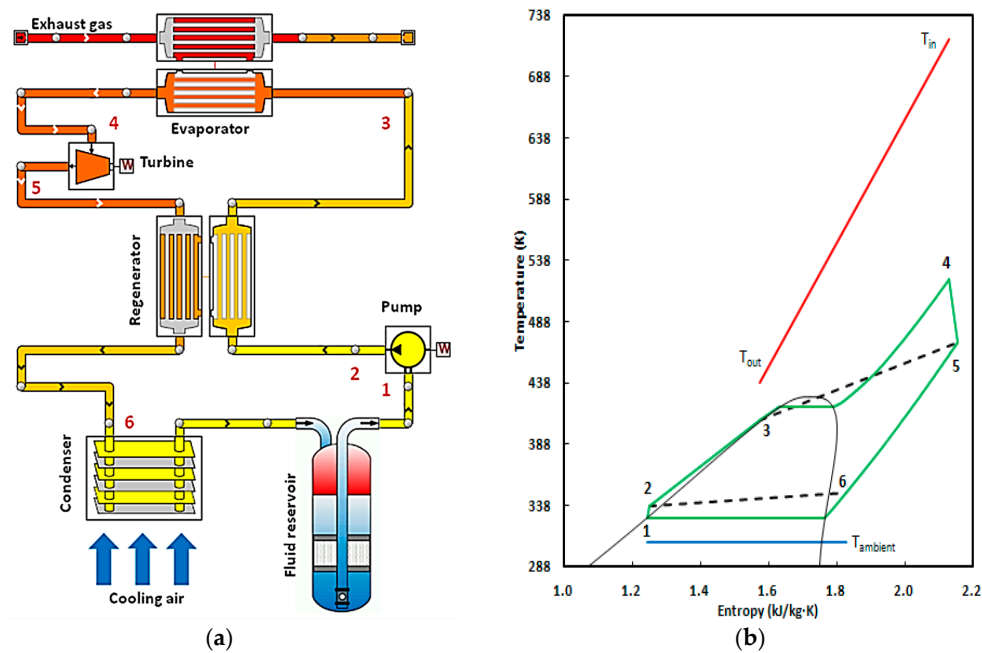
**Keywords:** organic Rankine cycle; radial turbine; similarity theory; entropy generation

## 1. Introduction

In recent years, automobile industry has made great progress in improving internal combustion engine thermal efficiencies. Current manufactured gasoline engines are working with maximum thermal efficiencies of 30%–36%, while diesel engines already reach 40%–47% [1]. Nowadays, the engine thermal efficiency is close to its technical limits but still not sufficient to meet future fuel economy targets without additional technologies. More than half of the fuel energy in the internal combustion engines is discharged in the form of heat to the environment. Waste heat recovery is considered as one of the most promising technologies to improve the engine thermal efficiency [2].

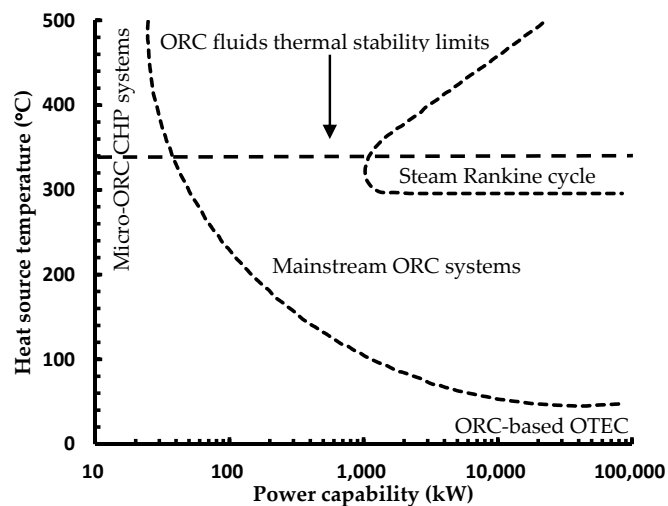
Several technologies can be applied to recover the waste heat of an internal combustion engine, including turbocompounding, organic Rankine cycle (ORC), and thermoelectric generators [3–6]. When comparing these technologies, two key factors should be taken into consideration. One is the utilization of the waste heat temperature range, the other is the efficiency improvement potentials. ORC can utilize all kinds of engine waste heat, and the engine BSFC saving potentials are very promising, around 5%–15% [7]. Hence, ORC is considered as the most appropriate waste heat recovery technology in the current conditions.

Figure 1 shows the demonstration of a regenerative organic Rankine cycle utilized for heavy-duty diesel engine exhaust gas recovery. The working fluid from the fluid reservoir is firstly pressurized by the working fluid pump, and then preheated in the regenerator by the high temperature working fluid out of the turbine. Secondly, the working fluid continues to be heated to the overheating state by the diesel engine high temperature exhaust gas, and then the superheating vapor enters into the turbine where it expands to the condensation pressure, during which mechanical work is transmitted to the application device through the shaft of the turbine. Finally, the working fluid is cooled sequentially in the regenerator and condenser to come back to the liquid state flowing into the fluid reservoir to complete the cycle.



**Figure 1.** Demonstration of a regenerative organic Rankine cycle for heavy-duty diesel engine exhaust gas heat recovery: (a) configuration of the regenerative organic Rankine cycle; and (b) T-s diagram of the regenerative organic Rankine cycle.

The use of organic fluids instead of water largely extends the application fields of Rankine cycle, making it promising especially in the low heat source temperature and small power size applications [8]. The Current and future ORC application fields versus steam Rankine cycle systems in terms of average temperature of the energy source and power capacity is shown in Figure 2. The steam Rankine cycle can be efficient only when the heat source temperature is above 300 °C and the system power capacity is above 1 MW. However, for ORC systems, the current application fields have extended to about 30 kW power capacities and 60 °C heat source temperatures. Two extreme applications are ORC based ocean thermal energy conversion (OTEC) for very low heat source temperatures and very large power capabilities, and micro-ORC combined heat and power (CHP) systems for very high heat source temperatures and very small power capabilities. The main advantages of ORC consist of two aspects [9]: (1) the working fluid can be an additional degree of freedom for a better design of the thermodynamic cycle for a specific heat source temperature, especially some of which are very efficient for low temperature applications; and (2) for the small power size applications, it is possible to design an efficient, reliable and cost-effective organic vapor expander. As for the heavy-duty diesel engine organic Rankine cycles, the power capacities are commonly within 30 kW, and heat source temperatures are either below 100 °C for engine coolant or above 400 °C for exhaust gases. As the core component of ORC systems, no efficient, reliable and cost-effective expanders can be found in the market until now for this specific application.



**Figure 2.** Current and future fields of application of ORC versus steam power systems in terms of average temperature of the energy source and power capacity [8].

Radial turbines are good candidates because of the advantages of small size, light weight, high design efficiencies, high reliability [10,11] and cost-effectiveness in mass productions. Many researchers have carried out studies related to the radial turbine design. As the organic fluid properties are totally different from air, these researches are mainly divided into two technical routes. One route focuses on forward design, including preliminary design of geometry parameters and aerodynamic design of blade profiles [12–21]. Dolz et al. [13] propose that the pre-design of turbomachinery must take real gas equations of state into consideration, because the specific energy deviation between real gas and perfect gas can be as large as 100%, which may lead to total wrong turbine preliminary design result. Fiaschi et al. [19,20] propose an accurate 0-D model to design low size radial ORC turbines. Different methods for the design of radial turbines were screened, with special attention paid to the estimation of losses. The results indicated that the total-to-total efficiencies of the designed turbines ranged from 72% to 80%. Costall et al. [21] also propose a detailed design methodology for ORC radial turbines. They used the methodology to design a radial turbine for the heavy-duty off-road diesel engine application. After three times of optimization, the best turbine produced 45.6 kW at 56.1% efficiency. Colonna et al. [16,17] made the fluid-dynamic design of ORC turbine using CFD tools. The authors numerically investigated the real gas effects occurring in the supersonic ORC stator nozzles. The results showed that a nozzle geometry with much higher exit-to-throat area ratio was required to obtain an efficient expansion. Wheeler and Ong [14,15] mainly focus on the radial turbine rotor flow mechanisms and geometry optimizations by the CFD tools. They suggested that small changes in the inducer shape had a significant effect on turbine efficiency due to the development of supersonic flows in the rotor. The strong interaction between the vane trailing-edge shocks and rotor leading-edge lead to a significant drop in efficiency, which should be specially considered.

The design and development of a turbine, which can be finally sold in the market, is a complex engineering problem involving turbine preliminary design, aerodynamic design of the blades, CFD analysis on the aerodynamic performance, rotor-dynamic analysis and system integration of turbine and auxiliary components [22]. In order to reduce the developmental effort involved in turbine preliminary design aspect, the other technical route is proposed to adapt an existing turbine using air as working fluid for ORC applications, namely similarity design [23–26]. Zhang et al. [24] established a performance prediction method from air to refrigerants taking compressibility factor into consideration. The results indicated that the relative deviation of main performance parameters at the design point working condition was no more than 5%, and under all working conditions were no more than 10%. White and Sayma [25] applied the similarity theory to predict turbine off-design performance over a

range of different operating conditions while utilizing different working fluids. The original similitude theory using turbine total inlet conditions was found to only apply within a small range of operating conditions, so a modified similitude theory was suggested that using the choked flow conditions instead. The results agreed with the CFD predictions within 2% for three organic fluids R245fa, R123 and R1234yf, right up until the choked mass flow rate. Wong and Krumdieck [26] scaled an industrial gas turbine to two refrigerants: R134a and R245fa. Three different approaches using the similarity theory were applied to scale the turbine performance map using air and generated the performance map for the two refrigerants. The results showed that the complete similarity could not be achieved for the same turbomachinery with two different working fluids, even at the best efficiency point. The authors indicated that the constant ratio of change of enthalpy to the squared of speed of sound in the turbine inlet approach would provide the highest accuracy in the performance estimation. The average errors of R134a and R245fa compared with air were 7.2% and 8.7%, respectively.

Until now, for the second technical route of turbine design, nearly all the literature focuses on the issue that finding an air turbine as the preliminary design result of organic fluids, but the issue of whether the aerodynamic design of blade profiles can adapt the new kind of working fluid has not been analyzed yet. That is to say, when a turbine using air as working fluid turns into using refrigerants as working fluids, how the turbine efficiency will change, and what loss mechanism differences lead to the efficiency change. It is very meaningful to answer this question, because the radial turbines using air as the working fluid in turbocharging applications have been very mature, and many technologies have been developed to improve the turbine efficiencies. It may largely shorten the time of aerodynamic design process of blade profiles of an ORC turbine when referring to the existing efficiency improving technologies.

In this paper, a radial turbine, for the heavy-duty diesel engine ORC application, is numerically simulated using R245fa and air as the working fluid to compare the differences of their performance and loss mechanism. R245fa, a typical organic fluid, is chosen as the working fluid because of its environmental friendly properties [27], good thermodynamic performance in the heavy-duty diesel engine applications [28] and high turbine nominal efficiency for small power size applications [20]. Firstly, the similarity criteria are deduced to obtain the similar operating condition between air and R245fa, and kinematic and dynamic similarities are verified. Then, the turbine performance maps are compared to find out the quantitative differences of total-to-static pressure ratio, reduced mass flow rate, reduced rotating speed and total-to-static isentropic efficiency. Finally, the similarities and differences of turbine entropy generation and loss mechanisms are discussed to explain the total-to-static isentropic efficiency difference.

## 2. Similarity Criteria

The general similarity criteria of turbines are summarized below, which can be found in the standard turbomachinery textbook [29].

- Flow coefficient

$$\Pi_1 = m / (\rho N D^3) \quad (1)$$

- Head coefficient

$$\Pi_2 = \Delta h_0 / U^2 \quad (2)$$

- Power coefficient

$$\Pi_3 = P / (\rho N^3 D^5) \quad (3)$$

- Reynolds number

$$\Pi_4 = \rho N D^2 / \mu \quad (4)$$

- Velocity ratio

$$\Pi_5 = U/C_s \quad (5)$$

Besides, the compressibility effect was proven to have large influence on the turbine efficiency. Usually, for the perfect gas the compressibility effect can be determined by the pressure ratio. However, based on the analysis of Macchi and Perdichizzi [30], for nonconventional fluids the associated similarity criterion of compressibility effect is volume expansion ratio, defined as the specific volume variation across the turbine in an isentropic process, which is applied instead of common characteristic parameter pressure ratio in this analysis.

- Compressibility coefficient

$$\Pi_6 = V_{out}/V_{in} \quad (6)$$

Air, which behaves like the perfect gas, obeys the perfect gas EoS like Equation (7), and the isentropic process obeys the following relationships (Equations (8) and (9)).

$$p = \rho RT \quad (7)$$

$$p_{in}/p_{out} = (\rho_{in}/\rho_{out})^\kappa \quad (8)$$

$$\Delta h_i = \frac{\kappa}{\kappa - 1} RT_{in} \left[ 1 - \left( \frac{p_{out}}{p_{in}} \right)^{\frac{\kappa-1}{\kappa}} \right] \quad (9)$$

The operating conditions of R245fa, including inlet pressure and temperature, rotating speed and outlet pressure, are obtained according to the thermodynamic analysis, and used as the input parameters to calculate all six similarity criteria (Equations (1)–(6)). Then, the similar operating conditions of air, including pressure ratio, rotating speed and inlet temperature, can be calculated in the following three steps.

- Pressure ratios in the air operating conditions can be obtained by Equations (6) and (8):

$$\frac{p_{in,a}}{p_{out,a}} = \Pi_6^\kappa \quad (10)$$

- Rotating speeds in the air operating conditions can be obtained by Equations (5), (9) and (10):

$$N = \frac{\Pi_5}{D} \sqrt{\frac{2\kappa}{\kappa - 1} RT_{in,a} (1 - \Pi_6^{1-\kappa})} \quad (11)$$

- Fluid dynamic viscosities are determined by the inlet operating conditions and associate similarity criteria, according to Equations (4), (7) and (11):

$$\mu = \frac{p_{in,a} \Pi_5 D}{\Pi_4} \sqrt{\frac{2\kappa}{(\kappa - 1) RT_{in,a}} (1 - \Pi_6^{1-\kappa})} \quad (12)$$

Given the turbine outlet pressure, on the one hand, the dynamic viscosity can be calculated by Equation (12), using inlet temperature as the only input variable; on the other hand, the dynamic viscosity can be obtained based on the air thermodynamic property tables when temperature and pressure are known. The result is that a unique inlet temperature can be solved to satisfy both Equation (12) and air thermodynamic property tables. Then, rotating speeds can be calculated based on Equation (11).

### 3. Numerical Method

The radial turbine in this study was applied for the heavy-duty diesel engine coolant heat recovery. The waste heat temperature is only 90 °C, and the quantity of heat in the design point is about 164 kW. The design operating pressure ratio is 2.5, and the associated output power is 10 kW. The turbine design parameters and geometry parameters are shown in Tables 1 and 2.

**Table 1.** Radial turbine design parameters.

Parameter	Value
Working fluid	R245fa
Inlet temperature (°C)	70
Inlet pressure (bar)	5.0
Outlet pressure (bar)	2.0
Output power (kW)	10
Design efficiency	80%

**Table 2.** Radial turbine geometry parameters.

Geometry Parameter	Value
Volute throat radius (mm)	129
Volute throat area (mm <sup>2</sup> )	1017
Nozzle inlet radius (mm)	100
Nozzle inlet vane angle (°)	70
Nozzle exit radius (mm)	84
Nozzle exit vane angle (°)	80
Number of nozzle vanes	15
Rotor inlet radius (mm)	82.5
Rotor inlet blade height (mm)	5
Rotor exit tip radius (mm)	50
Rotor exit hub radius (mm)	18
Rotor exit blade angle (°)	−55
Number of rotor blades	11

Three-dimensional steady computational fluid dynamics (CFD) simulations were carried out using the commercial code FINE<sup>TM</sup>/Open. FINE<sup>TM</sup>/Open is a Reynolds-average Navier-Stokes equation solver, which is based on the finite volume method, uses five stage explicit Runge-Kutta scheme and full hexahedra unstructured meshing strategy. The CFD domain consists of three components: the volute, full channels of nozzle ring and rotor wheel, which includes the exhaust pipe, as shown in Figure 3. A fine mesh of 13,782,018 grid points was generated. The mesh distribution was 1,274,890 grid points within the volute, 233,472 grid points per single channel nozzle ring passage, and 818,368 grid points per single channel rotor wheel and exhaust pipe passage. The grid independency study showed that the increase of grid points by 100% only made a 0.1% difference in the simulated total pressure loss through the volute and 0.08% difference in the simulated turbine total-to-static isentropic efficiency. It indicates that the discretization error is reduced to an acceptable error in the current grid point number.

The Helmholtz free energy equation of state fitted for organic fluid R245fa is utilized to calculate the gas properties. The estimated uncertainty for density is 0.1% in the liquid phase below 400 K with pressures up to 30 MPa. In the vapor phase and at temperatures above 400 K, the uncertainty is 1% in density, with higher uncertainties in the critical region. The uncertainty in vapor pressure is 0.2% above 250 K, and rises to 0.35% above 370 K [31]. The calculated thermodynamic properties were stored in the dedicated tables for the CFD code interpolation. The advantage of this approach is that no iterative inversion of the tables is done in the solver, therefore only a very small additional CPU time is needed. The bicubic interpolation approach was adopted to calculate values within the numerical interval.

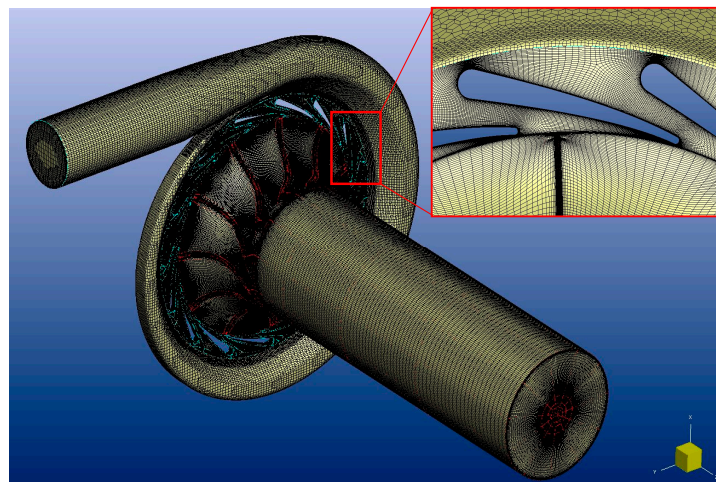


**Figure 3.** CFD domain including volute, full passages of nozzle ring, rotor wheel and exhaust pipe.

Total pressure and temperature with velocity normal to the volute inlet was used as the inlet boundary condition. The averaged static pressure was used as the outlet boundary condition. The non-matching frozen rotor method was adopted to deal with the interface between the stationary and rotating domain. All the walls were treated as smooth and adiabatic. Surface roughness can have influence on boundary layer growth and loss at high Reynolds numbers, and this assumption can be reasonable for new blades especially at low Reynolds numbers, the roughness of which is unknown [32]. Wall heat transfer is an important issue in the gas turbine airfoils simulations because of its extreme high temperature operating conditions and the adoption of blade cooling technology [33]. As for the ORC radial turbine, the operating temperature is low and no blade cooling technology is adopted, so the heat transfer through the wall should be very limited. When fixing all these settings, the selection of appropriate turbulence model was discussed. Four turbulence models were compared, which were Spalart-Allmaras (S-A), low Reynolds number  $k-\varepsilon$ ,  $k-\omega$  shear stress transport (SST), and explicit algebraic Reynolds stress model (EARSM) turbulence models. The 50% span blade-to-blade flow fields of absolute Mach number in the stationary domain (shown in Figure 4) and relative Mach number in the rotating domain (shown in Figure 5) are compared, respectively. The shock wave positions are almost the same for the four turbulence models, the main difference is value evaluation of absolute Mach number. When the result of  $k-\omega$  SST model is selected as the baseline, the difference of low Re  $k-\varepsilon$  model is almost zero. Spalart-Allmaras and EARSM models show smaller absolute Mach numbers in the shock wave position, but larger values near the leading edge of nozzle vanes. The difference values of EARSM model are generally smaller than those of Spalart-Allmaras model. As for the rotor separation flow simulation, using relative Mach number as the indicator, the separation flow in the suction side started earlier in most rotor wheel channels for Spalart-Allmaras model results. However, the phenomenon of separation flow starting earlier only happened in two or three rotor wheel channels in the low Re  $k-\varepsilon$  and EARSM models. In general, Spalart-Allmaras model shows the biggest difference compared with the other three models. For the other three turbulence models,  $k-\omega$  SST and EARSM turbulence models have almost the same isentropic efficiency simulation results, the difference of which is only 0.03%, 1% higher than low Re  $k-\varepsilon$  model result and 3% higher than Spalart-Allmaras model result. Based on the flow field and isentropic efficiency comparison results, the turbulence model used in this simulation is  $k-\omega$  SST model, which is also the commonly used two-equation turbulence model in the turbomachinery CFD simulation. The reasonability of these settings will be verified by the efficiency comparison between CFD simulations and experimental data.

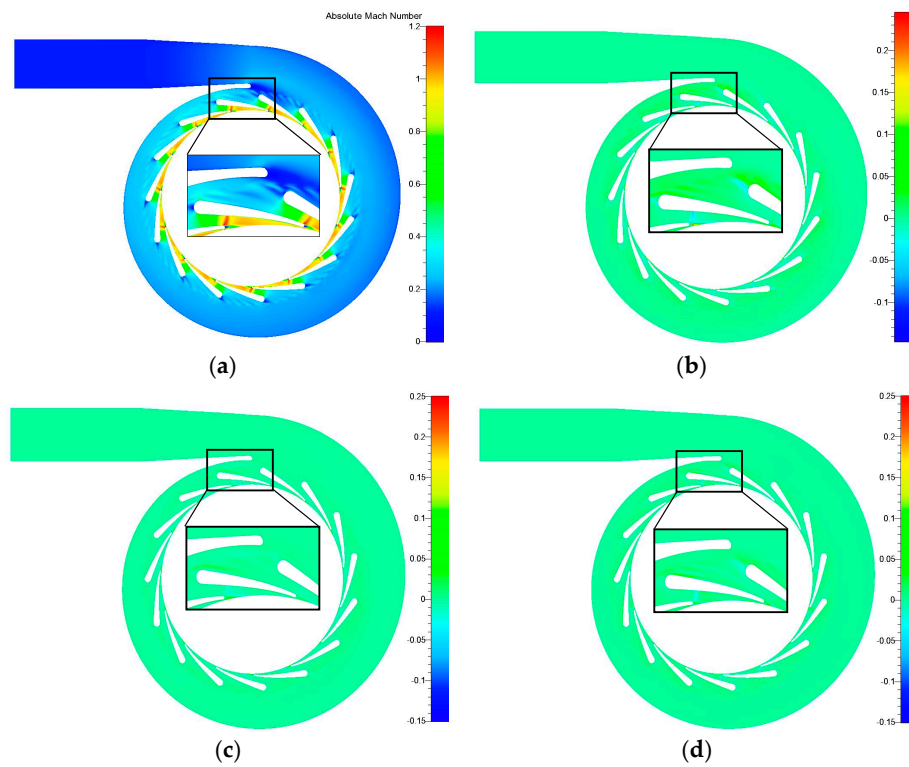


**Figure 4.** Absolute Mach number in the 50% span of stationary domain: (a) absolute Mach number value of k- $\omega$  SST model; (b) difference between S-A and k- $\omega$  SST model; (c) difference between low Re k- $\epsilon$  and k- $\omega$  SST model; and (d) difference between EARSM and k- $\omega$  SST model.

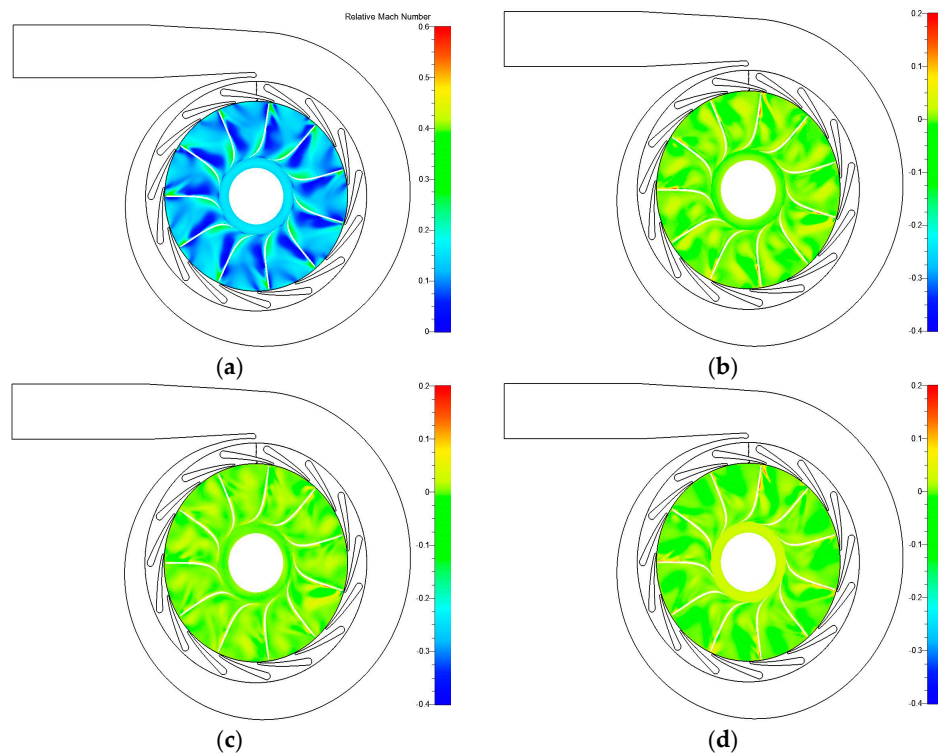


**Figure 5.** Relative Mach number in the 50% span of rotating domain: (a) relative Mach number value of k- $\omega$  SST model; (b) difference between S-A and k- $\omega$  SST model; (c) difference between low Re k- $\epsilon$  and k- $\omega$  SST model; and (d) difference between EARSM and k- $\omega$  SST model.

The numerical method in this study is verified using the available experimental data of Kang [34]. Table 3 shows CFD simulation results compared with literature experimental results. In this comparison, as the total parameters are used as inlet boundary conditions, so the static parameters have a little difference compared with the measured values. The efficiency comparison shows that the differences between simulation and experimental results for all the three operating conditions in the literature are within  $\pm 2.5\%$ . The simulation results based on the numerical method introduced above show acceptable agreements with the experimental results, and can be used for further discussions.

**Table 3.** Simulation results compared with literature experimental results.

Operating Condition	Comparison Parameter	CFD Value	Experimental Value
case 1	inlet temperature ( $^{\circ}\text{C}$ )	79.4	80.7
	inlet pressure (bar)	7.69	7.60
	outlet pressure (bar)	2.91	2.91
	isentropic efficiency	78.7%	76.0%
case 2	inlet temperature ( $^{\circ}\text{C}$ )	81.5	83.0
	inlet pressure (bar)	8.06	8.04
	outlet pressure (bar)	3.04	3.04
	isentropic efficiency	79.8%	77.5%
case 3	inlet temperature ( $^{\circ}\text{C}$ )	84.6	85.4
	inlet pressure (bar)	8.64	8.65
	outlet pressure (bar)	3.18	3.18
	isentropic efficiency	79.7%	82.2%

## 4. Results and Discussions

### 4.1. Turbine Performance Comparison

Kinematic and dynamic similarities of nominal and off-design operating conditions are verified according to the simulation results, as shown in Figure 6. Kinematic similarity is verified by absolute flow angle in the stationary domain and relative flow angle in the rotating domain, and dynamic similarity is verified by absolute Mach and Reynolds numbers in the stationary domain and relative values in the rotating domain.

For the flow angle comparison, almost all the differences in the stationary domain is zero, except for two positions. One is between the volute tongue and nearest nozzle vane leading edge, the other is at the nozzle vane trailing edges. In these locations, the largest absolute flow angle differences are about negative 10 degree for the nominal condition and 15 degree for the off-design condition. In the rotating domain, most relative flow angle differences are within  $\pm 10$  degree for the nominal condition and  $\pm 15$  degree for the off-design condition, except for the separation flow region. The flow in this region is disordered, and flow angles change a lot for the reason of some complicated fluid motion like backflow.

For the Mach number comparison, the agreement in the flow field is quite well. Almost all the differences are around zero, the differences can be observed within  $-0.05$  to  $0.10$  only in limited regions at the nozzle throat and near the rotor blade surfaces. For the Reynolds number comparison, the main differences occur within the latter half of the nozzle passage, which is the transonic and supersonic region in the nozzle flow field. The Reynolds number in the air condition in this region is about 10% larger than that in the R245fa condition, mainly because the absolute velocity values of air are larger than those of R245fa in the transonic and supersonic region. However, Reynolds number values in these positions are so large that their influence on the performance of similar operating conditions will be very limited.

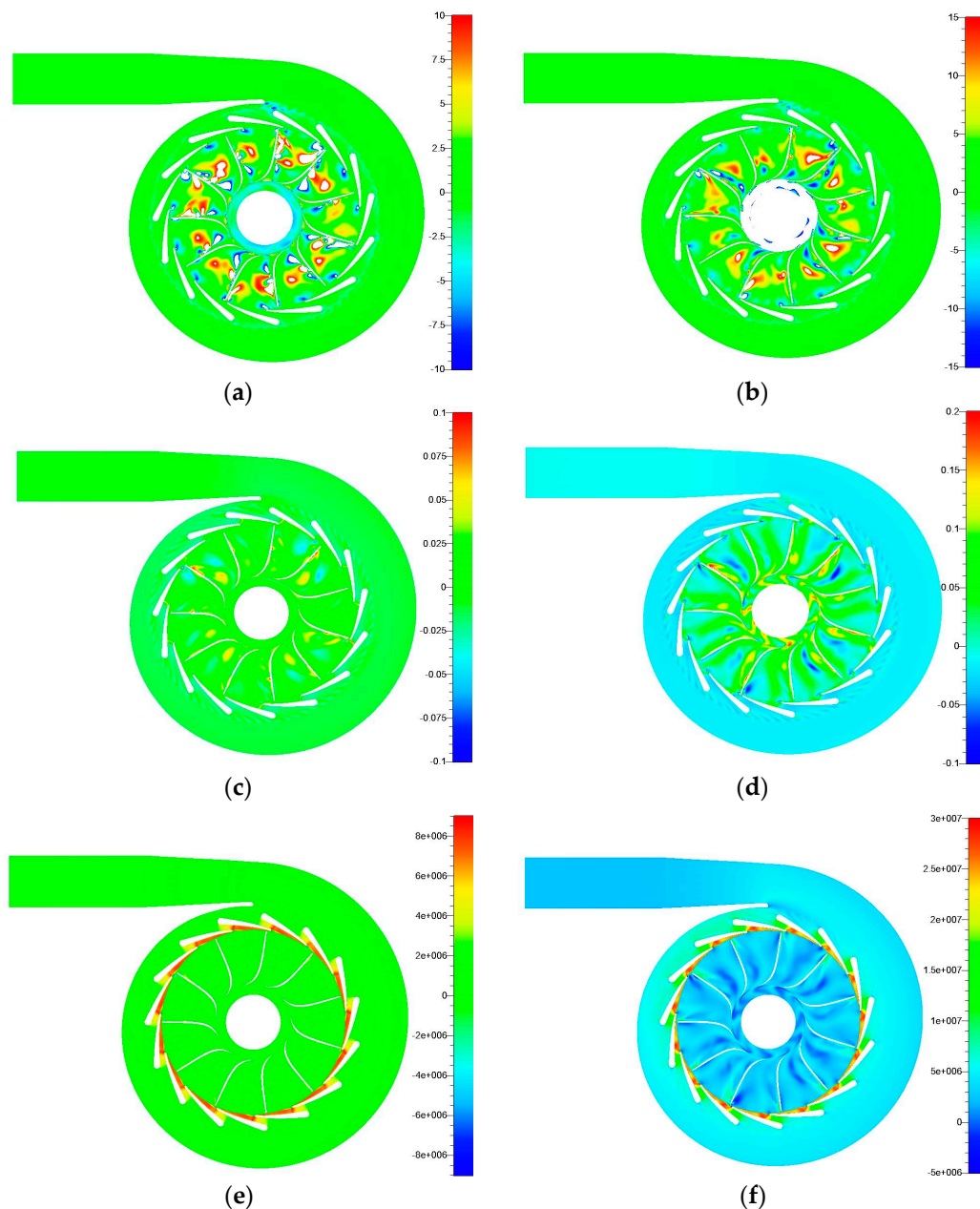


**Figure 6.** Kinematic and dynamic similarity verification at the nominal and off-design operating conditions: (a) flow angle differences between air and R245fa at the nominal condition; (b) flow angle differences between air and R245fa at the off-design condition; (c) mach number differences between air and R245fa at the nominal condition; (d) mach number differences between air and R245fa at the off-design condition; (e) reynolds number differences between air and R245fa at the nominal condition; and (f) reynolds number differences between air and R245fa at the off-design condition.

The comparison results indicate that the dynamic similarity is in good agreement, but the kinematic similarity is not as well as dynamic similarity. In some small regions, the kinematic similarity may not perform well, but, in most regions, the kinematic similarity is still in good agreement. Figure 7 shows the influence of kinematic similarity differences on the turbine efficiency evaluations. The parameter difference in percentage terms is defined as  $(\text{value}_{\text{air}} - \text{value}_{\text{R245fa}}) / \text{value}_{\text{R245fa}}$ . Based on the similarity criteria deduced in Section 2, the relative flow angle in the rotating domain in the air conditions are larger than those in the R245fa conditions. For most conditions, the simulated efficiencies in the air conditions are also larger. When discussing the relationship between kinematic

similarity criteria difference and efficiency difference, the trend line indicate that the increase of kinematic similarity criteria differences may lead to the slight increase of turbine efficiency difference, but the effect is limited. In general, the similarity criteria can be good enough for the similar operating condition calculation from R245fa to air.

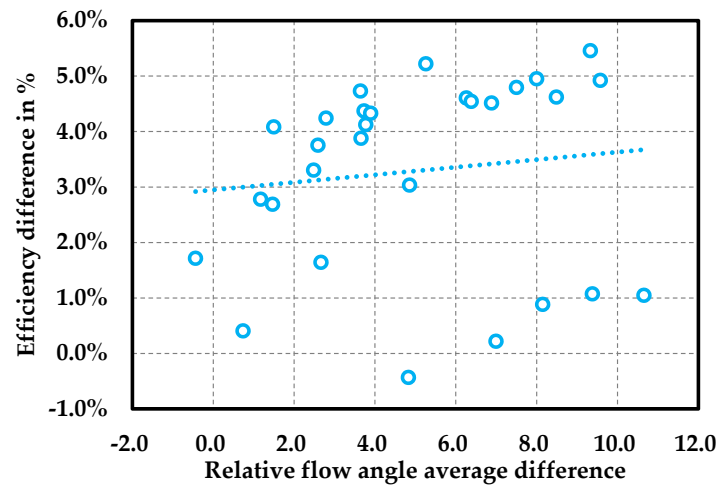


**Figure 7.** Total-to-static isentropic efficiency difference in percentage terms compared with the relative flow angle average difference.

Several reduced and non-dimensional parameters are very important when analyzing a turbine performance. They are total-to-static pressure ratio, reduced rotating speed, reduced mass flow rate, and total-to-static isentropic efficiency. Based on the similarity criteria deduced, all these turbine performance parameters, except isentropic efficiency, are mainly related to three characteristic parameters, which are turbine compressibility coefficient  $\Pi_6$  and working fluid properties, including specific heat ratio  $\kappa$  and gas constant  $R$ . The relationship between pressure ratio and characteristic parameters is shown in Equation (10). The other two relationships are shown below:

$$N_{reduced} = \frac{N}{\sqrt{T_{in}}} \propto \sqrt{\frac{2\kappa}{\kappa-1} R (1 - \Pi_6^{1-\kappa})} \quad (13)$$

$$m_{reduced} = \frac{m\sqrt{T_{in}}}{p_{in}} \propto \sqrt{\frac{2\kappa}{\kappa-1} \frac{1}{R} (1 - \Pi_6^{1-\kappa})} \quad (14)$$

Figure 8 shows the turbine performance maps using R245fa and air as working fluid respectively. For total-to-static pressure ratio comparison, the results in the air operating conditions are larger than those in the R245 conditions, mainly because of larger specific heat ratio of air. In general, in the simulation operating conditions, specific heat ratios of R245fa are within 1.10 to 1.25, and that of air is 1.4. As the volume expansion ratio increases, the pressure ratio in the air condition increases a lot. When the volume expansion ratio is 5.78, the pressure ratio of R245fa in this condition is only 5.5, but that of air exceeds 11, more than twice larger. As for the reduced rotating speed and mass flow rate, gas constant is another important impact factor. The gas constant of air is 287.1 J/(kg·K), and that of R245fa is only 62.02 J/(kg·K). Because the gas constant of air is much larger than that of R245fa, it will dominate the magnitude relationship of reduced rotating speed and mass flow rate between air and R245fa. The qualitative results are that reduced rotating speeds of air operating conditions are larger than those of R245fa conditions, and the reduced mass flow rates of air operating conditions are smaller than those of R245fa conditions. In all the simulated operating conditions, the ratios of reduced rotating speed and mass flow rate between R245fa and air are nearly constant. The values of reduced rotating speed in the R245fa conditions are about 0.4 of those in air conditions, and the values of reduced mass flow rate in R245fa conditions are about twice of those in air conditions. The reason is

that although volume expansion ratio increases a lot, the ratio of  $(1 - \Pi_6^{1-\kappa})$  between two working fluids changes only a little, and thus the ratios of these two turbine performance parameters are almost constant. Isentropic efficiency cannot be directly discussed in this way because it is non-dimensional. The turbine efficiency map in Figure 8b indicates that the use of R245fa will decrease the turbine isentropic efficiencies. In the high efficiency region, where velocity ratio is around 0.7, the efficiency decrease can be as much as 4%.

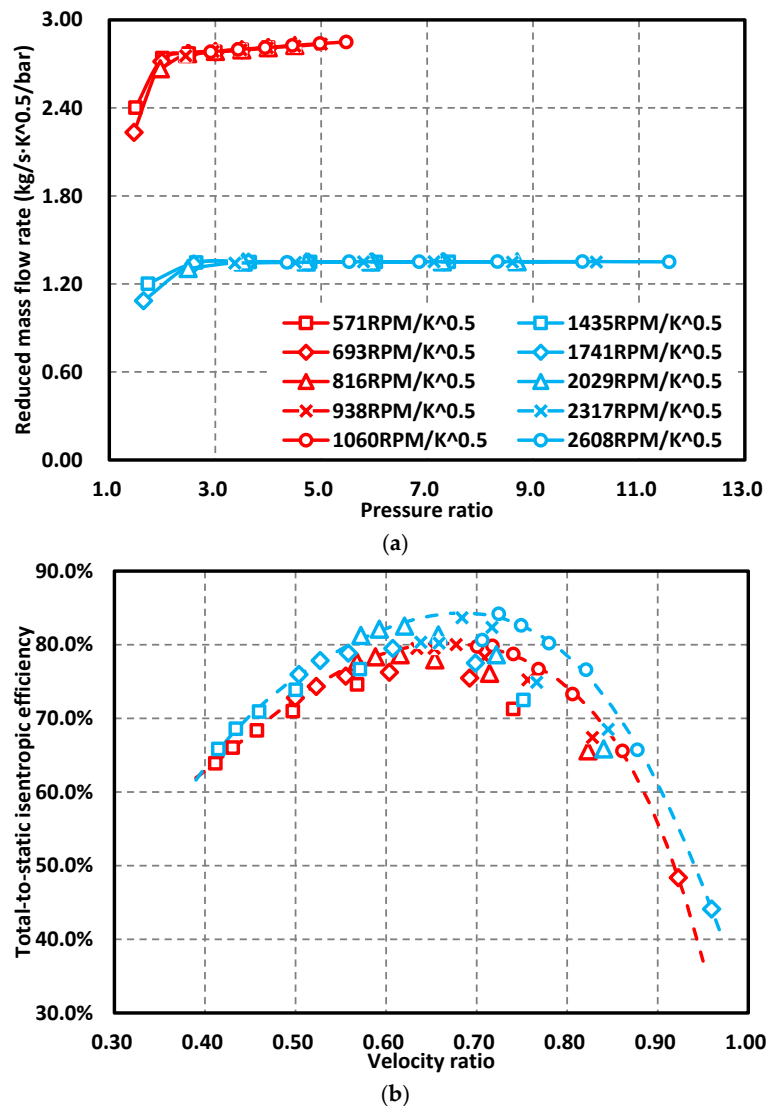


**Figure 8.** Turbine performance map comparison between R245fa (in red color) and air (in blue color): (a) reduced mass flow rates versus total-to-static pressure ratios at five reduced rotating speeds; and (b) total-to-static isentropic efficiencies versus velocity ratios.

#### 4.2. Turbine Loss Mechanisms Comparison

Efficiency is probably the most important performance parameter for the turbomachinery. This is especially true for organic Rankine cycle turbines because the system net output power is directly related to the difference between the turbine work and pump work. Denton [35] points out that the most rational measure of loss generation in an adiabatic turbomachinery is by the form of entropy generation. Entropy generation rate is a useful concept, and as the CFD simulation tools developed a lot during the last decades, it is convenient to be calculated now. Since 2000, several researchers have reported the turbine loss mechanisms by the concept of entropy generation rates [36,37].

The entropy generation rate per unit mass in a fluid can be analytically derived from the equations of conservation of momentum and energy along with the second law of thermodynamics, as shown by Greitzer et al. [38]. This derivation form is expressed as followed:

$$\frac{Ds}{Dt} = \frac{Q}{T} - \frac{1}{\rho T} \frac{\partial q_i}{\partial x_i} + \frac{1}{\rho T} \tau_{ij} \frac{\partial u_i}{\partial x_j} \quad (15)$$

where  $\tau_{ij}$  is the viscous stress tensor, defined according to Newton's laws of viscous:

$$\tau_{ij} = \mu \left( \frac{\partial u_i}{\partial x_j} + \frac{\partial u_j}{\partial x_i} \right) + \delta_{ij} \lambda \nabla \cdot \mathbf{u} \quad (16)$$

where  $\lambda$  is the second viscosity that relates stresses to the volumetric deformation, and Stokes hypothesis of  $\lambda = -2/3\mu$  is frequently used, which was found to be a good approximation for gases.

As the turbine flow is assumed to be adiabatic, the first term in Equation (15) on the right hand side can be ignored. For the Reynolds-average Navier–Stokes equation solver, the other two terms can be further expressed as Equation (17) according to Moore and Moore's analysis [39,40]. They first developed an expression for entropy generation rate per unit volume, applying the Reynolds decomposition for temperature and velocity.

$$\overline{T} s_v = \frac{k}{\overline{T}} \left[ \left( \frac{\partial \overline{T}}{\partial x_i} \right)^2 + \left( \frac{\partial T'}{\partial x_i} \right)^2 \right] + \overline{\tau}_{ij} \frac{\partial \overline{u}_i}{\partial x_j} + \overline{\tau'_{ij}} \frac{\partial u'_i}{\partial x_j} \quad (17)$$

where Moore and Moore used the eddy viscosity to model the turbulent viscous dissipation:

$$\overline{\tau'_{ij}} \frac{\partial u'_i}{\partial x_j} = \frac{\mu_t}{\mu} \overline{\tau}_{ij} \frac{\partial \overline{u}_i}{\partial x_j} \quad (18)$$

Martinez-Botas et al. [38] assumed that the effect of thermal diffusion could be negligible compared to the generation of entropy through turbulent viscous dissipation in the turbine adiabatic flow process. Hence, the current used form of entropy generation rate per unit volume can be defined as Equation (19). All the variables in the equation can be obtained in the CFD post process.

$$s_v = \frac{1}{\overline{T}} \left( \overline{\tau}_{ij} \frac{\partial \overline{u}_i}{\partial x_j} + \frac{\mu_t}{\mu} \overline{\tau}_{ij} \frac{\partial \overline{u}_i}{\partial x_j} \right) \quad (19)$$

Figures 9 and 10 illustrate the flow fields of the normalized entropy generation rate per unit volume on the hub (10% span), midspan (50% span) and shroud (90% shroud) blade-to-blade surfaces of stationary and rotating domain in the nominal and off-design conditions. In general, the large entropy generation regions are similar between R245fa and air simulation results, and also similar between nominal and off-design operating conditions. Almost all the losses are within the nozzle ring and rotor wheel flow fields.

In the nozzle ring, there exist three kinds of losses. The first one is in the suction side near leading edge of several nozzle vanes. The general fluid flow direction is close to the vane surface in the nozzle. However, in the large entropy generation region near the leading edges, the fluid flow direction is away from the vane suction surface. The fluid is firstly separated from the suction surface near the leading edge, and then attaches to the suction surface in the middle of vane chord. It is mainly caused by the non-uniform flow direction out of the volute, and thus leads to the flow direction departure from the vane surfaces because of flow interaction within the neighboring several nozzle vanes. The second one is in the throat of the nozzle passage, where the transonic flow occurs. The losses are mainly caused by the shock waves. The third loss is the nozzle vane trailing edge loss. The loss is caused by the detached vortex just after the vane trailing edge when the fluid flow over the nozzle vane.

A couple of symmetric vortex is generated in this place, and leading to a low velocity but large entropy generation region.

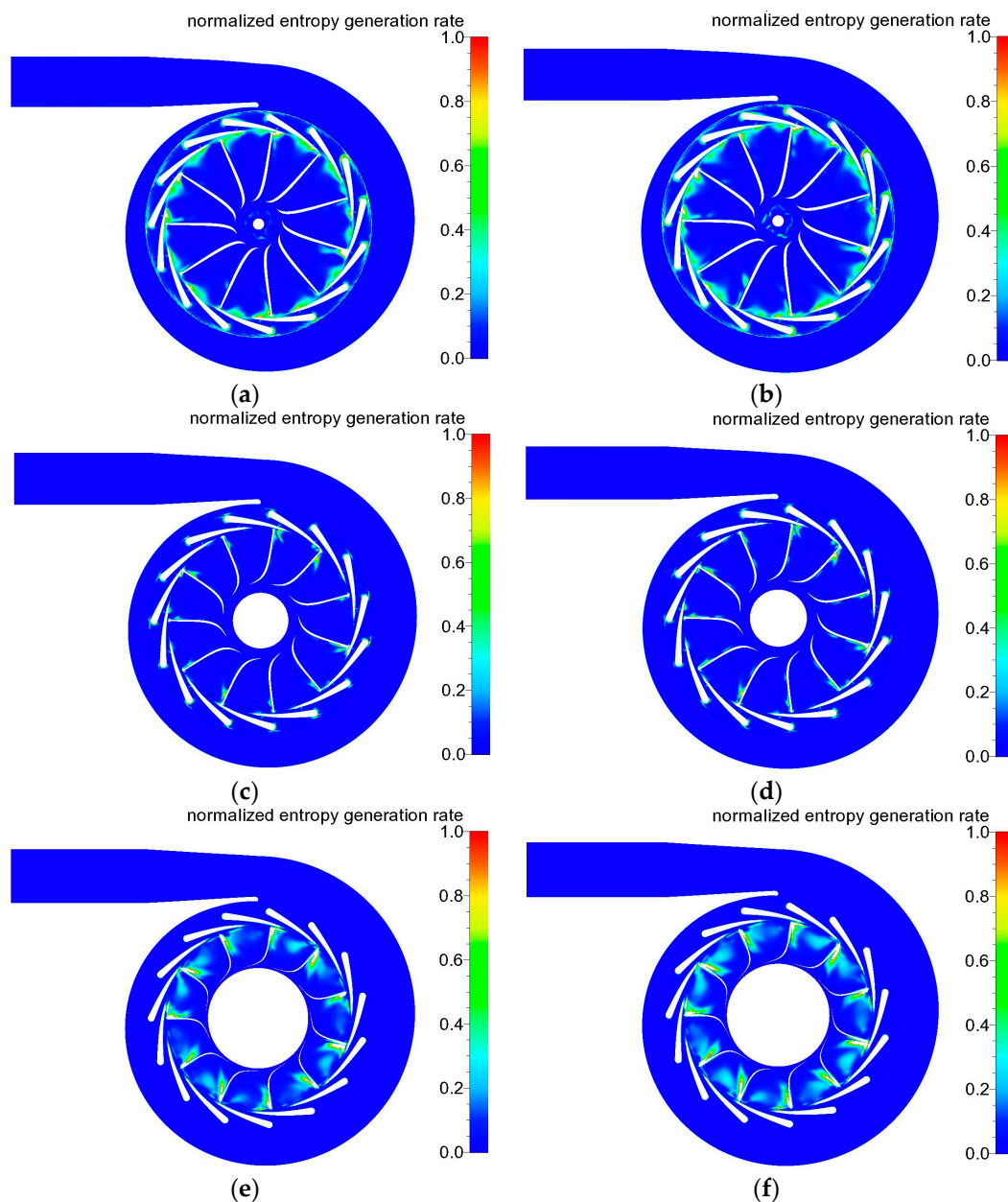


**Figure 9.** Entropy generation rate per unit volume in the nominal operating condition: (a) 10% span of blade-to-blade surface flow field of 245fa case; (b) 10% span of blade-to-blade surface flow field of air case; (c) 50% span of blade-to-blade surface flow field of 245fa case; (d) 50% span of blade-to-blade surface flow field of air case; (e) 90% span of blade-to-blade surface flow field of 245fa case; and (f) 90% span of blade-to-blade surface flow field of air case.

As for the rotor wheel passage, the losses are much larger than those in the nozzle vane passage. Three losses dominate the large entropy generation in the rotor passage. Near the hub surface, it is obvious that the entropy generation is very large in the region, where the low velocity fluids after the nozzle trailing edges just flow into the rotor passage. The reason of this kind of loss is that when the low absolute velocity fluid flows into the rotor, its local relative flow angle is nearly negative  $90^\circ$ . This value is much larger than the average rotor inlet relative flow angle as well as the recommended

optimal relative flow angle, and thus leads to very large incidence loss. The second large entropy generation region is caused by the fluid boundary layer separation on the suction surface of rotor blades, generating near the leading edge and developing to the latter half of the blades, which can be observed in Figures 9d and 10d. The last large entropy generation region is also in the rotor inlet but near the shroud surface. This is an unshrouded radial turbine, so the fluid moves from the pressure surface to the suction surface through the tip clearance. The tip leakage fluids perform like a jet flow, and mix with the main stream on the suction surface near the shroud surface. Hence, it leads to a large entropy generation region near the leading edge on the blade suction surface.

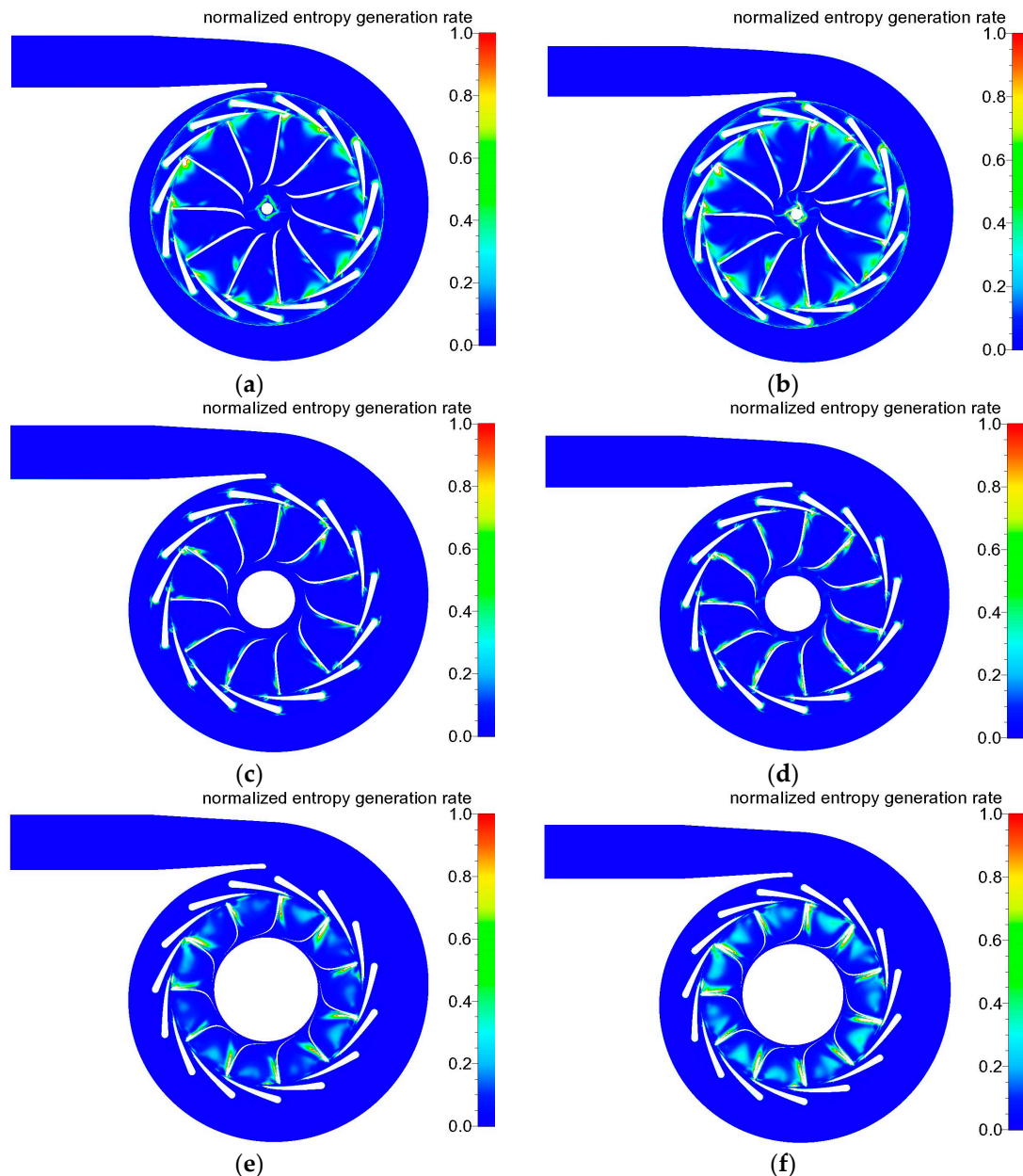


**Figure 10.** Entropy generation rate per unit volume in the off-design operating condition: (a) 10% span of blade-to-blade surface flow field of 245fa case; (b) 10% span of blade-to-blade surface flow field of air case; (c) 50% span of blade-to-blade surface flow field of 245fa case; (d) 50% span of blade-to-blade surface flow field of air case; (e) 90% span of blade-to-blade surface flow field of 245fa case; and (f) 90% span of blade-to-blade surface flow field of air case.

In all these losses, some behavior is almost the same between R245fa and air, such as separation and attachment flow on the suction surface of nozzle vanes, the nozzle vane trailing edge losses caused by symmetric detached vortex, incidence losses and tip clearance leakage losses in the rotor passage. That is to say, for the losses mentioned above, optimization technologies can be universal for radial turbine both using R245fa and air as working fluids. However, the optimization of two losses should take working fluid properties into consideration, which are shock wave loss in the nozzle passage and boundary layer separation loss on the rotor blade suction surface. They are also the important reasons leading to the isentropic efficiency difference between R245fa and air, as shown in Figure 8b.

Compared with air results, the maximum absolute Mach numbers in the nozzle passage of R245fa are smaller both in the nominal and off-design operating conditions, as shown in Table 4. In the off-design condition, the maximum absolute Mach number of R245fa is 1.58, but that of air is 1.70. Smaller absolute Mach number will weaken the shock wave losses occurring in the throat of nozzle passage. Total pressure loss coefficient  $\zeta$  is used for nozzle loss comparison, which is defined as

$$\zeta = 1 - \frac{p_{total, nozzle outlet}}{p_{total, volute outlet}} \quad (20)$$

**Table 4.** The maximum absolute Mach number and total pressure loss coefficient in the nozzle ring.

Operating Condition	Absolute Mach Number		Total Pressure Loss Coefficient	
	R245fa	Air	R245fa	Air
nominal	1.23	1.28	6.0%	7.2%
off-design	1.58	1.70	7.9%	8.9%

The results in the nominal and off-design conditions indicate that the nozzle passage losses of R245fa are smaller than those of air. The difference is about 1%. Figure 11 shows that the flow field from throat to outlet of the nozzle passage is already supersonic. The shock wave location estimation is the same for the two working fluids, mainly from the trailing edge of suction surface to the perpendicular position on the pressure surface. The shock wave strength is different. It is obvious that the shock wave using air as working fluid is stronger, and thus larger shock wave losses.

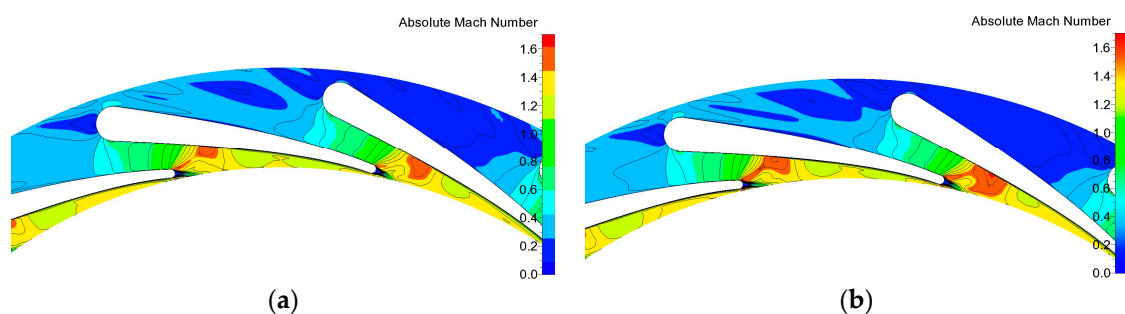


**Figure 11.** Absolute Mach number distribution in the nozzle ring at off-design operating condition: (a) R245fa case; and (b) air case.

When comparing the separation loss on the blade suction surface in the rotor passage, normalized pressure both on the rotor blade pressure and suction surfaces along the meridional length for R245fa and air in the nominal and off-design operating conditions are shown in Figure 12. Small pressure increase is observed for air conditions along the blade suction surface. This increase is associated with the adverse pressure gradient near the leading edge of the suction surface, which is caused by the fluid of large positive incidence angle near the leading edge separating from the suction surface. The leading edge separation for R245fa is weaker, as shown from the suction surface pressure

distribution. However, stronger separation can be observed for R245fa compared with air in the middle of the suction surface, as shown in Figure 13, which is the velocity streamline and relative Mach number distributions on the rotor midspan blade-to-blade surface. Larger low relative Mach number region exists on the suction surface between blade leading and trailing edge when using R245fa as working fluid. Finally it leads to the results that the average pressure differences between pressure and suction surfaces for R245fa are about 33% smaller than those for air both in the nominal and off-design conditions. The results from efficiency performance and loss mechanism comparison indicate that when using R245fa as working fluid, it will decrease the shock wave loss, but increase the rotor boundary layer separation loss, and eventually decrease the turbine isentropic efficiency.

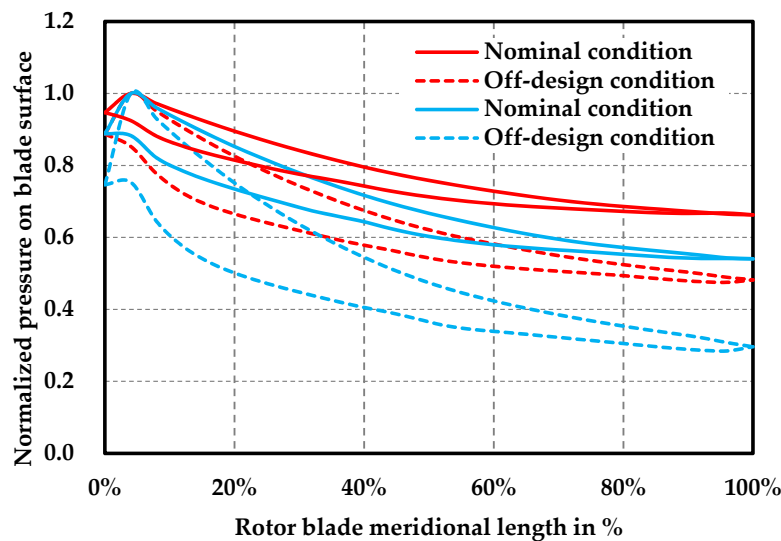


**Figure 12.** Normalized pressure comparison along the meridional length both on blade pressure and suction surfaces between R245fa (in red color) and air (in blue color).

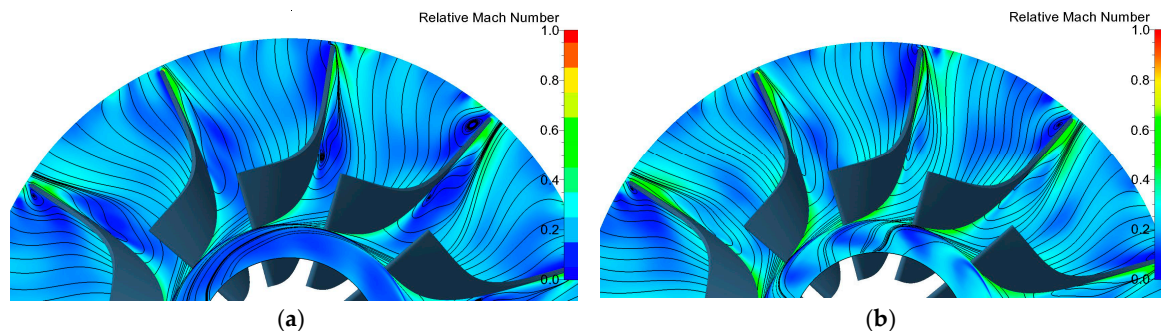


**Figure 13.** Velocity streamline and relative Mach number distribution in the rotor wheel at off-design operating condition: (a) R245fa case; and (b) air case.

## 5. Conclusions

In this paper, the performances of a radial turbine applied for heavy-duty diesel engine ORC systems are numerically simulated using R245fa and air as working fluid based on the similarity theory, and the turbine performance and loss mechanism differences are compared between these two working fluids. The results indicate the following conclusions.

Based on the built similarity criteria, the working fluid properties of specific heat ratio and gas constant have clear relationships with the turbine performance parameters, including total-to-static pressure ratio, reduced rotating speed and mass flow rate. As both specific heat ratio and gas constant of R245fa are smaller, the total-to-static pressure ratios for R245fa operating conditions are smaller

than those for air conditions: the reduced rotating speeds of R245fa are 0.4-fold of those of air, and the reduced mass flow rates of R245fa are twice as many as those of air.

Turbine total-to-static isentropic efficiencies in the velocity ratio from 0.5 to 0.9 are more than 70% no matter using R245fa or air as the working fluid. Entropy generation rate per unit volume is introduced as the indicator to analysis the loss mechanisms. Six losses dominate the turbine efficiency decreasing: flow separation on the nozzle vane suction surface near the leading edge, shock wave loss in the throat of nozzle passage, symmetric detached vortex loss after the nozzle vane trailing edge, local incidence loss near the rotor hub surface, boundary layer separation vortex loss on the blade suction surface in the rotor passage, and tip leakage loss near the rotor shroud surface.

The nozzle throat shock wave and rotor passage separation vortex loss comparison between R245fa and air are analyzed deeply. The maximum absolute Mach numbers in the nozzle for R245fa are smaller than those for air, leading to about 1% of total pressure loss coefficient decrease. However, the rotor passage separation vortex for R245fa is larger, which eventually decreases the turbine isentropic efficiency. In general, the air turbine efficiencies are 3%–4% larger than those of the R245fa turbine in the velocity ratio between 0.5 and 0.9.

In the future, turbine rotor blades optimization based on the organic working fluid properties will be discussed in detail to decrease the rotor passage separation vortex and improve the organic fluid radial turbine efficiencies.

**Acknowledgments:** The authors would like to thank the National Natural Science Foundation of China (No. 51636005) for the support.

**Author Contributions:** Lei Zhang and Tao Chen deduced the similarity criteria and performed the CFD simulations. Lei Zhang, Weilin Zhuge and Yangjun Zhang analyzed the simulation results and wrote the paper. All authors contributed equally for reviewing and revising the paper. All authors have read and approved the final manuscript.

**Conflicts of Interest:** The authors declare no conflict of interest.

## Nomenclature

$C_s$	velocity if working fluid expansion in an ideal nozzle	m/s
$D$	rotor diameter	m
$N$	rotating speed	RPM
$P$	power	kW
$Q$	heat amount	W
$R$	gas constant	J/(kg·K)
$T$	temperature	K
$U$	circumferential velocity	m/s
$V$	volume flow rate	m <sup>3</sup> /s
$h$	specific enthalpy	J/kg
$m$	mass flow rate	kg/s
$p$	pressure	Pa
$s$	specific entropy	J/(kg·K)

## Greek Symbols

$\kappa$	specific heat ratio	
$\lambda$	second viscosity	Pa·s
$\mu$	dynamic viscosity	Pa·s
$\xi$	total pressure loss coefficient	
$\rho$	density	kg/m <sup>3</sup>
$\tau$	viscous stress tensor	

## Subscripts

0	total parameter
a	air related parameter
in	inlet parameter
org	organic fluid related parameter
out	outlet parameter
t	turbulence parameter

## References

1. Boretti, A.A. Energy recovery in passenger cars. *J. Energy Resour. Technol.* **2012**, *134*, 022203. [[CrossRef](#)]
2. Stanton, D.; Charlton, S.; Vajapeyazula, P. Diesel engine technologies enabling powertrain optimization to meet U.S. greenhouse gas emissions. *SAE Int. J. Engines* **2013**, *6*, 1757–1770. [[CrossRef](#)]
3. Saidur, R.; Rezaei, M.; Muzammil, W.K.; Hassan, M.H.; Paria, S.; Hasanuzzaman, M. Technologies to recover exhaust heat from internal combustion engines. *Renew. Sustain. Energy Rev.* **2012**, *16*, 5649–5659. [[CrossRef](#)]
4. Zhao, R.; Zhuge, W.; Zhang, Y.; Yin, Y.; Zhao, Y.; Chen, Z. Parametric study of a turbocompound diesel engine based on an analytical model. *Energy* **2016**, *115*, 435–445. [[CrossRef](#)]
5. Armstead, J.R.; Miers, S.A. Review of waste heat recovery mechanisms for internal combustion engines. *J. Therm. Sci. Eng. Appl.* **2014**, *6*, 014001. [[CrossRef](#)]
6. Ringler, J.; Seifert, M.; Guyotot, V.; Hübner, W. Rankine cycle for waste heat recovery of IC engines. *SAE Int. J. Engines* **2009**, *2*, 67–76. [[CrossRef](#)]
7. Sprouse, C.; Depcik, C. Review of organic Rankine cycles for internal combustion engine exhaust waste heat recovery. *Appl. Therm. Eng.* **2013**, *51*, 711–722. [[CrossRef](#)]
8. Gaia, M. 30 Years of ORC Development. In Proceedings of the 1st International Seminar on ORC Power Systems (ORC2011), Delft, The Netherlands, 22–23 September 2011.
9. Colonna, P.; Casati, E.; Trapp, C.; Mathijssen, T.; Larjola, J.; Turunen-Saaresti, T.; Uusitalo, A. Organic Rankine cycle power systems: From the concept to current technology, applications, and an outlook to the future. *J. Eng. Gas Turbines Power* **2015**, *137*, 100801. [[CrossRef](#)]
10. Bao, J.; Zhao, L. A review of working fluid and expander selections for organic Rankine cycle. *Renew. Sustain. Energy Rev.* **2013**, *24*, 325–342. [[CrossRef](#)]
11. Quoilin, S.; Broek, M.V.D.; Declaye, S.; Dewallef, P.; Lemort, V. Techno-economic survey of Organic Rankine Cycle (ORC) systems. *Renew. Sustain. Energy Rev.* **2013**, *22*, 168–186. [[CrossRef](#)]
12. Kang, S.H.; Chung, D.H. Design and Experimental Study of Organic Rankine Cycle (ORC) and Radial Turbine. In Proceedings of the ASME 2011 Turbo Expo: Turbine Technical Conference and Exposition, Vancouver, BC, Canada, 6–10 June 2011.
13. Luján, J.M.; Serrano, J.R.; Dolz, V.; Sánchez, J. Model of the expansion process for R245fa in an Organic Rankine Cycle (ORC). *Appl. Therm. Eng.* **2012**, *40*, 248–257. [[CrossRef](#)]
14. Wheeler, A.P.S.; Ong, J. A Study of the Three-dimensional Unsteady Real-gas Flows within a Transonic ORC Turbine. In Proceedings of the ASME Turbo Expo 2014: Turbine Technical Conference and Exposition, Düsseldorf, Germany, 16–20 June 2014.
15. Dur’a Galiana, F.J.; Wheeler, A.P.S.; Ong, J. A Study of Trailing-edge Losses in Organic Rankine Cycle Turbines. In Proceedings of the ASME Turbo Expo 2015: Turbine Technical Conference and Exposition, Montréal, QC, Canada, 15–19 June 2015.
16. Colonna, P.; Harinck, J.; Rebay, S.; Guardone, A. Real-gas effects in organic Rankine cycle turbine nozzles. *J. Propuls. Power* **2008**, *24*, 282–294. [[CrossRef](#)]
17. Harinck, J.; Turunen-Saaresti, T.; Colonna, P.; Rebay, S.; Buijtenen, J.V. Computational study of a high-expansion ratio radial organic Rankine cycle turbine stator. *J. Eng. Gas Turbines Power* **2010**, *132*, 054501. [[CrossRef](#)]
18. Turunen-Saaresti, T.; Tang, J.; Buijtenen, J.V.; Larjola, J. Experimental and Numerical Study of Real-Gas Flow in a Supersonic ORC Turbine Nozzle. In Proceedings of the ASME Turbo Expo 2006: Power for Land, Sea, and Air, Barcelona, Spain, 8–11 May 2006.
19. Fiaschi, D.; Manfrida, G.; Maraschiello, F. Thermo-fluid dynamics preliminary design of turbo-expanders for ORC cycles. *Appl. Energy* **2012**, *97*, 601–608. [[CrossRef](#)]
20. Fiaschi, D.; Manfrida, G.; Maraschiello, F. Design and performance prediction of radial ORC turboexpanders. *Appl. Energy* **2015**, *138*, 517–532. [[CrossRef](#)]
21. Costall, A.W.; Gonzalez Hernandez, A.; Newton, P.J.; Martinez-Botas, R.F. Design methodology for radial turbo expanders in mobile organic Rankine cycle applications. *Appl. Energy* **2015**, *157*, 729–743. [[CrossRef](#)]
22. Japikse, D.; Baines, N.C. *Introduction to Turbomachinery*; Concepts NREC: Corporate Headquarters 217 Billings Farm Road White River Junction, VA, USA, 1995.
23. Zhang, L.; Zhuge, W.L.; Zheng, X.Q.; Zhang, Y.J. The Influence of Working Fluid Characteristic Parameters on Turbine Performance for the Small Scale ORC system. In Proceedings of the ASME 2013 Fluids Engineering Division Summer Meeting, Incline Village, NE, USA, 7–11 July 2013.

24. Chen, T.; Zhuge, W.L.; Zhang, L.; Zhang, Y.J. Similarity based performance prediction of organic rankine cycle turbine using air condition data. In Proceedings of the ASME-JSME-KSME 2015 Joint Fluids Engineering Conference, Seoul, Korea, 26–31 July 2015.
25. White, M.; Sayma, A.I. The application of similitude theory for the performance prediction of radial turbines within small-scale low-temperature organic Rankine cycles. *J. Eng. Gas Turbines Power* **2015**, *137*, 122606. [[CrossRef](#)]
26. Wong, C.S.; Krumdieck, S. Scaling of gas turbine from air to refrigerants for organic rankine cycle using similarity concept. *J. Eng. Gas Turbines Power* **2015**, *138*, 061701. [[CrossRef](#)]
27. Calm, J.M.; Hourahan, G.C. Physical, Safety, and Environmental Data for Current and Alternative Refrigerants. In Proceedings of the 23rd International Congress of Refrigeration, Prague, Czech Republic, 21–26 August 2011.
28. Teng, H.; Regner, G.; Cowland, C. *Waste Heat Recovery of Heavy-Duty Diesel Engines by Organic Rankine Cycle Part II: Working Fluids for WHR-ORC*; SAE Technical Paper 2007-01-0543; SAE World Congress & Exhibition: Detroit, MI, USA, 16–19 April 2007.
29. Mousapha, H.; Zelesky, M.F.; Banies, N.C.; Japikse, D. *Axial and Radial Turbines*; Concepts NREC: Corporate Headquarters 217 Billings Farm Road White River Junction, VA, USA, 2003.
30. Macchi, E.; Perdichizzi, A. Efficiency prediction for axial-flow turbines operating with nonconventional fluids. *J. Eng. Power* **1981**, *103*, 718–724. [[CrossRef](#)]
31. Lemmon, E.W.; Span, R. Short fundamental equations of state for 20 industrial fluids. *J. Chem. Eng. Data* **2006**, *51*, 785–850. [[CrossRef](#)]
32. Denton, J.D. Some limitations of turbomachinery CFD. In Proceedings of the ASME Turbo Expo 2010: Power for Land, Sea, and Air, Glasgow, UK, 14–18 June 2010.
33. Harrison, K.L.; Bogard, D.G. Use of the adiabatic wall temperature in film cooling to predict wall heat flux and temperature. In Proceedings of the ASME Turbo Expo 2008: Power for Land, Sea, and Air, Berlin, Germany, 9–13 June 2008.
34. Kang, S.H. Design and experimental study of ORC (organic Rankine cycle) and radial turbine using R245fa working fluid. *Energy* **2012**, *41*, 514–524. [[CrossRef](#)]
35. Denton, J.D. Loss mechanisms in turbomachines. *J. Turbomach.* **1993**, *115*, 621–656. [[CrossRef](#)]
36. Pullan, G.; Denton, J.; Curtis, E. Improving the Performance of a Turbine with Low Aspect Ratio Stators by Aft-Loading. *J. Turbomach.* **2006**, *128*, 492–499. [[CrossRef](#)]
37. Newton, P.; Copeland, C.; Martinez-Botas, R.; Seiler, M. An audit of aerodynamic loss in a double entry turbine under full and partial admission. *Int. J. Heat Fluid Flow* **2012**, *33*, 70–80. [[CrossRef](#)]
38. Greitzer, E.M.; Tan, C.S.; Graf, M.B. *Internal Flow: Concepts and Applications*; Cambridge University Press: Cambridge, UK, 2004.
39. Moore, J.; Moore, J.G. Entropy production rates from viscous flow calculations Part I—A turbulent boundary layer flow. In Proceedings of the ASME 1983 International Gas Turbine Conference and Exhibit, Phoenix, AZ, USA, 27–31 March 1983.
40. Moore, J.; Moore, J.G. Entropy production rates from viscous flow calculations Part II—Flow in a rectangular elbow. In Proceedings of the ASME 1983 International Gas Turbine Conference and Exhibit, Phoenix, AZ, USA, 27–31 March 1983.

